

Experimental Investigations of Polymer Hollow Fibre Heat Exchangers for Building Heat Recovery Application

Xiangjie Chen¹, Yuehong Su¹, Devrim Aydin¹, David Reay², Richard Law², Saffa Riffat¹

¹Department of Architecture and Built Environment, University of Nottingham, University Park, NG7 2JQ, Nottingham. United Kingdom

²David Reay & Associates, United Kingdom

Contact: Xiangjie Chen; Email:xiangjie.chen@nottingham.ac.uk

Abstract: Due to low cost, light weight and corrosion resistant features, polymer heat exchangers have been extensively studied by researchers with the aim to replace metallic heat exchangers in a wide range of applications. Although the thermal conductivity of polymer material is generally lower than the metallic counterparts, the large specific surface area provided by the polymer hollow fibre heat exchanger (PHFHE) offers the same or even better heat transfer performance with smaller volume and lighter weight compared with the metallic shell-and-tube heat exchangers. This paper presents the construction and experimental investigations of polypropylene based polymer hollow fibre heat exchangers in the form of shell-and-tube. The measured overall heat transfer coefficients of such PHFHEs are in the range of 258-1675W/m²K for water to water application. The effects of various parameters on the overall heat transfer coefficient including flow rates and numbers of fibres, the effectiveness of heat exchanger, the number of heat transfer unit (NTU), and the height of transfer unit (HTU) are also discussed in this paper. The results indicate that the PHFHEs could offer a conductance per unit volume of 4*10⁶W/m³K, which is 2~8 times higher than the conventional metal heat exchangers. This superior thermal performance together with its low cost, corrosive resistant and light weight features make PHFHEs potentially very good substitutes for metallic heat recovery system for building application.

Key words: Polymer hollow fibre, heat recovery, heat exchanger, heat transfer, experimental testing

Nomenclature

A Heat transfer area (m²)

C_p Specific heat (J/Kg K)

CUV Conductance per unit volume (W/m³K)

D Tube/shell diameter (m)

Gz Graetz number

HTU Height of transfer unit (m or cm)

k Thermal conductivity (W/mK)

L Length (m)

36	\dot{m}	Mass flow rate (kg/s)
37	N	Number of fibres inside the heat exchanger
38	NTU	Number of heat transfer unit
39	Nu	Nusselt number
40	ΔP	Pressure drop (Pa)
41	Pr	Prandtl number
42	Q	Heat transfer rate (W)
43	\dot{V}	Volumetric flow rate (m ³ /s)
44	R	Thermal resistance (m ² /KW)
45	Re	Reynolds number
46	St	Stanton number
47	T	Temperature (°C)
48	U	Overall heat transfer coefficient (W/m ² K)
49	V	Volume (m ³)

50

51 **Greek Letters/Subscripts**

52	α	Surface to volume ratio (m ² /m ³)
53	c,i	Cold side inlet
54	c,o	Cold side outlet
55	ε	Heat exchanger effectiveness
56	i	Inside
57	λ	Packing fraction of a PHFHE equals to ND_0^2/D_S^2
58	h,i	Hot side inlet
59	h,o	Hot side outlet
60	lm	Logarithmic mean
61	o	Outside
62	ov	Overall
63	ρ	Density of the fluid (kg/m ³)
64	s	Shell side

65	t	Tube side
66	u	Linear velocity inside the tube (m/s)
67	μ	Dynamic viscosity of the fluid(kg/ms)
68	w	Wall

69 1. Introduction

70 In the era of rapid global economic development, the growing world energy use has triggered
71 problems such as primary energy supply difficulties and world-wide environmental concerns
72 (carbon emission, global warming, air pollution, etc). In developed countries, the energy
73 consumption of buildings account for 20-40% of the total final energy consumption¹. Heat
74 recovery systems² in the form of air ventilation systems³⁻⁵, membrane heat exchangers^{6,7},
75 metal heat exchanger^{8,9} have been extensively studied by researchers with the aim to improve
76 energy efficiency and reduce energy costs for building applications. Most of such heat
77 recovery systems are made from metallic materials, which have the disadvantages in terms of
78 weight and cost. In addition, specially treated metal heat exchanger is needed if the working
79 fluids are corrosive. Moreover, the manufacturing process of metal materials consumes
80 significant amount of primary energies, accompanied by carbon emissions. Given these
81 considerations, it is desirable to find an alternative material for heat exchangers that can
82 overcome these disadvantages and also acquire comparable heat exchange efficiency and be
83 easily fabricated. This is where the use of polymer heat exchanger comes into place. With the
84 advantages of greater fouling and corrosion resistance, greater geometric flexibility and ease
85 of manufacturing, reduced energy of formation and fabrication, and the ability to handle
86 liquids and gases (i.e, single and two-phase duties), polymer heat exchangers have been
87 widely studied and applied in the field of evaporative cooling system^{10,11}, micro-electronic
88 cooling devices^{12,13}, water desalination systems^{14,15}, solar water heating systems^{16,17}, liquid
89 desiccant cooling systems^{18,19}, etc. The detailed research progresses and various applications
90 of polymer hollow fibre heat exchanger can be found in the review paper²⁰. Most importantly,
91 polymer materials can offer substantial weight, space, and volume savings, which make them
92 more competitive compared with heat exchangers manufactured from many metallic alloys.
93 Moreover, the energy required to produce a unit mass of polymers is about two times lower
94 than common metals, making them environmentally attractive²¹.

95 One of the drawbacks of polymer materials are their relatively low thermal conductivities,
96 typically in the range of 0.1 to 0.4 W/m²K, which is about 100-200 times lower than the
97 metal materials. In order to overcome this obstacle and increase the thermal performance of
98 polymer heat exchanger, researchers have studied the polymer heat exchangers with various
99 configurations: gas to air heat exchanger with triangular channels²², shell and tube or
100 immersion coil fluoropolymer heat exchanger²³, air to water heat exchanger with rectangular
101 channel plate²⁴, plastic falling-film evaporator²⁵. But the overall heat transfer coefficients
102 achieved were still very low, which were in the range of 341-567 W/m²K, with the fibre
103 outside diameter between 2.54mm and 9.53mm.

104 The relatively low overall heat transfer coefficients can be improved and reach values
105 comparable to metal heat exchangers, when the heat exchanger is made from polymer micro-
106 hollow fibre with fibre wall thickness below $100\mu\text{m}$ ²⁵. Several researches have been focused
107 on the heat transfer mechanism of polymer micro-hollow fibre heat exchangers (PHFHE),
108 with inside and outside diameter (ID and OD) less than 0.1mm. Bourouni et al.²⁶ presented
109 experimental data on a falling film evaporator and condenser made of 2.5 cm diameter
110 circular PP tubes (wall thickness of 5 mm) used in an ‘aero-evapo-condensation process’ for
111 desalination. The results showed that for the same thermal performance, such polymer heat
112 exchanger was 2-3 times cheaper than its metal counterpart. Zarkadas and Sirkar²⁷ reported
113 polymeric hollow fibre heat exchangers (PHFHE) for low temperature (up to 150-200°C)
114 applications. The overall heat transfer coefficients for the water-water, ethanol-water, and
115 steam-water systems reached 647-1314, 414-642, and 2000 W/(m²K), respectively. An
116 olefin/paraffin distillation system using hollow fibre structured packings (HFSP) was
117 proposed by Yang et al.²⁸. This group of researchers recently scaled up the experiment and
118 long-term operational testing results were obtained and reported (Yang et al.²⁹). The results
119 demonstrated that after long-term exposure to light hydrocarbon environments ($\leq 70^\circ\text{C}$), the
120 mechanical properties of the PP polymer did not degrade significantly. Astrouski I. et al.³⁰
121 studied the fouling effect of polymeric heat exchanger made from PP (inner and out fibre
122 diameter of 0.461mm and 0.523mm respectively) for the purpose of cooling TiO₂ suspension.
123 The experimental test results showed a very high overall heat transfer coefficient, with up to
124 2100W/m²K for clean conditions and 1750W/m²K for dirty conditions at the flow velocity of
125 0.05m/s. Zhao et al.³¹ presented a numerical analysis of a novel PP hollow fibre heat
126 exchanger for low temperature applications using FLUENT. The heat transfer coefficient of
127 PP fibres was predicted to be achieved at 1109W/m²K with inside and outside fibre diameters
128 of 0.6mm and 1mm respectively.

129 The lack of extensive experience and testing data for polymer hollow fibre plastic heat
130 exchanger and the unwillingness of industry partners to depart from well established metal
131 heat exchanger remain to be big barriers for the wide applications of this technology. With
132 the aim to experimentally investigate the effects of various working flow rates and number of
133 fibres on the overall heat transfer coefficients, and to validate the theoretical simulation
134 model developed by the authors, three different modules of polymer hollow fibre heat
135 exchanger (fibre ID of 450 μm and OD of 550 μm) were fabricated and tested in the laboratory
136 testing conditions. The effects of various parameters on the overall heat transfer coefficient
137 including flow rates, numbers of fibres, the effectiveness of heat exchanger, the number of
138 heat transfer unit (NTU), and the height of transfer unit (HTU) are discussed in this paper.
139 The experimental obtained overall heat transfer coefficient and overall conductance per unit
140 volume for PHFHE are compared with these of metal heat exchangers. The experimental
141 uncertainties occurred associated with the measurement of flow rates and working fluid
142 temperatures, etc. are also analysed.

143

144 2. Theory

145 Assuming there is no heat loss to the surrounding, the overall heat transfer rate Q , between
 146 the shell side and tube side fluids, is defined by the flow rates of the hot and cold fluids flow
 147 rates and their inlet and outlet temperatures, as shown in the following equation:

$$148 \quad Q = \dot{m}_t c_{p,t} (T_{c,o} - T_{c,i}) = \dot{m}_s c_s (T_{h,i} - T_{h,o}) \quad \text{Eq. (1)}$$

149 Where subscript t denotes tube side and s denotes shell side.

150 The overall heat transfer coefficient U , can be given by:

$$151 \quad U = Q / (A \Delta T_{lm}) \quad \text{Eq. (2)}$$

152 Where Q is an average heat transfer rate value between two fluids;

153 A is the heat transfer area (for hollow fibre heat exchanger, A is the total inside surface area
 154 of the hollow fibres);

155 ΔT_{lm} is the logarithmic mean temperature difference (LMTD), and is defined as:

$$156 \quad \Delta T_{lm} = \frac{\Delta T_1 - \Delta T_2}{\ln[\Delta T_1 / \Delta T_2]} \quad \text{Eq. (3)}$$

157 Here ΔT_1 and ΔT_2 are the temperature differences between two fluids at each end of a
 158 heat exchanger. In our case, for counter-flow heat exchanger

$$159 \quad \Delta T_1 = T_{h,i} - T_{c,o} \quad \Delta T_2 = T_{h,o} - T_{c,i} \quad \text{Eq. (4)}$$

160 The heat exchanger effectiveness ε , number of transfer unit (NTU) and the height of transfer
 161 unit (HTU) can be calculated using the following equations³²:

$$162 \quad \varepsilon = \frac{U_i A_i \Delta T_{lm}}{C_{min} (T_{h,i} - T_{c,i})} \quad \text{Eq. (5)}$$

$$163 \quad NTU = \frac{U_i A_i}{C_{min}} = \frac{U_o A_o}{C_{min}} \quad \text{Eq. (6)}$$

$$164 \quad HTU = L / NTU \quad \text{Eq. (7)}$$

165 Where L is the length of the heat exchanger and C_{min} is given by:

$$166 \quad C_{min} = \{\dot{m}_t c_t, \dot{m}_s c_s\}_{min} \quad \text{Eq. (8)}$$

167 The performance comparison between PHFHEs and existing metal heat exchangers should be
 168 made on a volumetric basis, so the so-called overall conductance per unit volume¹⁴ (CUV) is
 169 defined, which is the product of the heat transfer coefficient and the surface to volume ratio α :

$$170 \quad CUV = \alpha U \quad \text{Eq. (9)}$$

171 CUV in this case expresses the total amount of heat transferred per unit time and unit volume.
172 A higher CUV value indicates a more compact heat exchanger which can offer the same
173 thermal performance, or a heat exchanger that transfers more heat for the same heat
174 exchanger volume.

175 The surface to volume ratio α of the PHFHE is the ratio between the fibre inside area to the
176 volume of the heat exchanger, which can be calculated by:

$$177 \quad \alpha = \frac{A_i}{V} = \frac{4ND_i}{D_s^2} \quad \text{Eq.(10)}$$

178 In fluid dynamics, the Graetz number (Gz) is a dimensionless number that
179 characterizes laminar flow in a conduit. This number is useful in determining the thermally
180 developing flow entrance length in ducts. As stated by Hewit et al.³³, small values of Gz (Gz
181 < 20) indicates that radial temperature profiles are fully developed inside the laminar flow
182 tube. The Gz number is defined as:

$$183 \quad G_z = \frac{D_H}{L} Re Pr \quad \text{Eq.(11)}$$

184 Where

185 D_H is the diameter in round tubes or hydraulic diameter in arbitrary cross-section ducts (m);

186 L is the length;

187 Re is the Reynolds number and

188 Pr is the Prandtl number.

189

190 The theoretical tube side pressure drop for a PHFHE can be calculated based on Darcy-

191 Weisban Equation as stated by³⁴:

$$192 \quad \Delta P = fL \frac{\rho u^2}{2d_h} \quad \text{Eq.(12)}$$

193 Where f is the flow resistance, also known as friction factor;

194 ΔP is the pressure drop of the tube side for PHFHE;

195 ρ is the density of the water.

196 The shell side and tube side Reynolds number are calculated using following equation:

$$197 \quad Re = \frac{D * G}{\mu} \quad \text{Eq. (13)}$$

198 Where, D is fiber inside/outside diameter for tube/shell side Reynolds number;

199 μ is dynamic viscosity of the tube/shell side fluid for tube/shell side Reynolds number ;

200 G is fluid mass velocity at the center line of the heat exchanger, detailed calculations could
201 be referred to Kern³⁵.

202 The relationship between the tube side Reynolds number and tube side linear velocity is
203 described by Kern³⁵ as following:

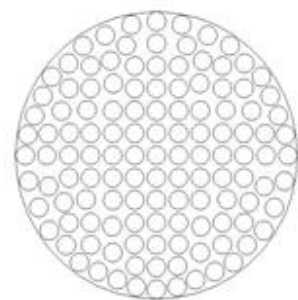
$$204 \quad Re_t = \frac{\rho * D_t * u_t}{\mu} \quad \text{Eq. (14)}$$

205 The relationship between the shell side Reynolds number³⁵ and shell side linear velocity can
206 be found in³⁵ as following:

$$207 \quad Re_s = \frac{\rho * D_o * u_s}{\mu} \quad \text{Eq. (15)}$$

208 3. Apparatus and procedure

209 Polypropylene (PP) hollow fibres (manufactured by ZENA Ltd.) with outside diameter of
210 550 μ m and inside diameter of 450 μ m were used for the fabrication of three modules, with
211 their geometrical information listed in Table 1. The shell side tube diameter was 15mm for
212 Module 1 and Module 2 and 22mm for Module 3. The three modules were fabricated in
213 following way: The two ends of the fibres in a bundle were glued together first using PTFE
214 resin. The fibre bundle was then inserted into a plastic tubing which was connected by two
215 tee fittings, as shown in Figure 1. The fibre bundle was sealed with the two ends of the plastic
216 tubing and the excessive length of fibres was cut. The two ends of the plastic tubing can be
217 connected with a water loop, so they serve as the inlet and outlet of one water flow. **The tube**
218 **side hot water and shell side cooling water are in the counter flow direction.** The detailed
219 images and testing rig of PHFHE modules could be found in Figure 1.



220
221 A: PHFHE heat exchanger (fibre number: 100 and 200)

B: PHFHE heat exchanger cross section view (not to scale)

222 Figure 1-a PHFHE heat exchanger

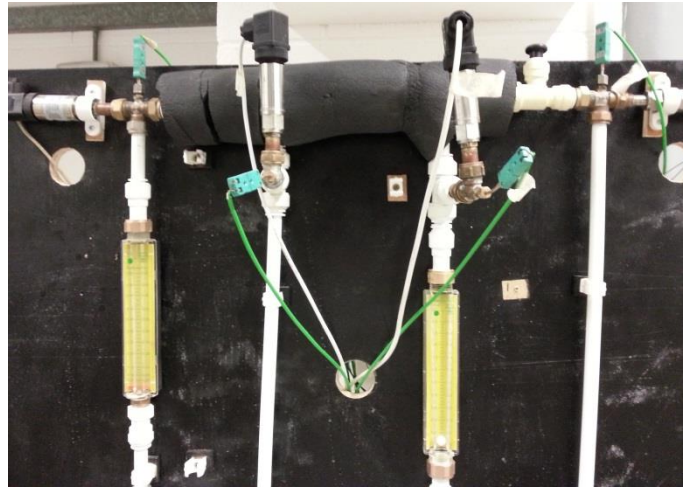


Figure 1-b PHFHE heat transfer measurement testing rig

Table 1 Geometrical Characteristic of PHFHE

Module	Fibre number (N)	Active Length (cm)	Total Length (cm)	λ	Ao (cm ²)	α
1	100	14.0	21.5	0.135	242	889
2	200	14.0	21.5	0.269	484	1778
3	400	14.0	21.5	0.538	968	3556

The schematic diagram of the experimental testing rig for the heat transfer measurement is shown in Figure 2. A 10 kW electric heater which could provide hot water up to 80° C, was used to provide hot water for the PHFHE module. Each time before starting the test, the heater was pre-setted to the required testing hot water condition. As soon as the hot water temperature reached the desired testing value, the test was ready to start. In order to remove any particulate matter and avoid blocking the hollow fibres, two micro filters (5 µm) for both shell and tube sides were introduced before hot water and cooling water entering into the PHFHE. The hot water feed was then introduced to the shell side of the PHFHE module from the electric heater by a centrifugal pump at a constant flow rate (0.1-0.6l/min) which was controlled by a ball valve. Tap water with the temperature around 14-16°C was used as the cooling water, which passed through the shell side of the PHFHE at constants flow rates (0.2-2.0l/min) controlled by a ball valve. In all runs, the hot water and cooling water went in counter flow directions. The inlet and outlet temperatures and pressures of two streams were measured by K type thermocouples and pressure sensors (Ge UNIK 5000) with the accuracy of ±0.2% and ±0.5% respectively.

The experimental procedures applied for the tests are as following: Firstly the hot water flow rate was maintained at a fixed value, while the cooling water flow rates were varied from 0.2-2.0l/min with 0.2l/min increments. Temperatures of the inlet and outlet of the two streams were recorded every 10 seconds by a DT800Data taker, until two to five subsequent readings did not differ by more than ±0.1°C. The hot water inlet temperature was varied between 38 °C to 69 °C, while the cooling water inlet temperature was kept between 14°C and 16°C.

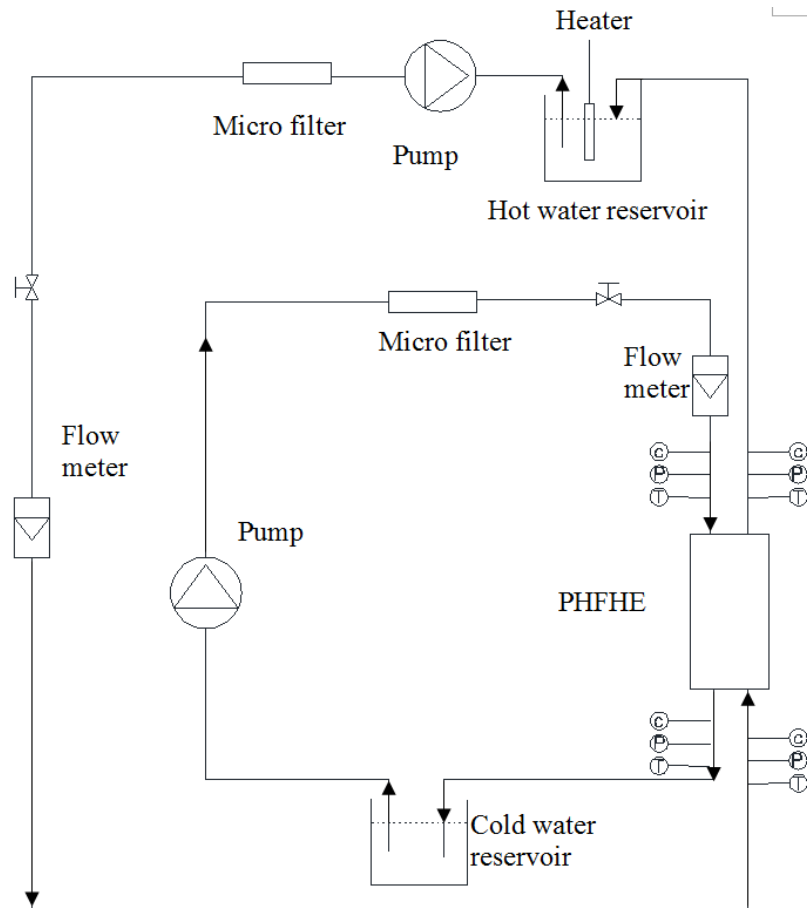


Figure 2 The experimental schematic diagram for heat transfer measurements in PHFHE

4. Results and Discussion

In order to obtain the overall heat transfer coefficients, the heat transfer rate Q should be determined by the mass flow rate and the temperature difference for the tube side or shell side. Figure 3 presents the experimentally obtained overall heat transfer coefficients under the conditions when the tube side flow rate was 0.5l/min, and the shell side flow rates were varied between 0.2l/min and 2.0l/min. It can be found that when the shell side flow rate is less than 0.8l/min, the overall heat transfer coefficient calculated from the thermal capacity change Q_h of tube side is higher than that calculated from the thermal capacity change Q_c of shell side. When the shell side flow rate is higher than 0.8l/min, the situation is reversed. The difference between the U values calculated from the respective change of the thermal capacity of two streams tends to increase largely as the shell side flow rate increases. However, the difference of the U values obtained by two streams is less than 10%, with the discrepancy being amplified by the fact that very low flow rate was applied in the tube side. As the shell side is well thermally insulated, heat loss may have a smaller effect on this discrepancy. So, in order to compensate and reduce the discrepancy, the average Q values between the two streams are used for the following analysis and discussions, as presented in the rest of the paper.

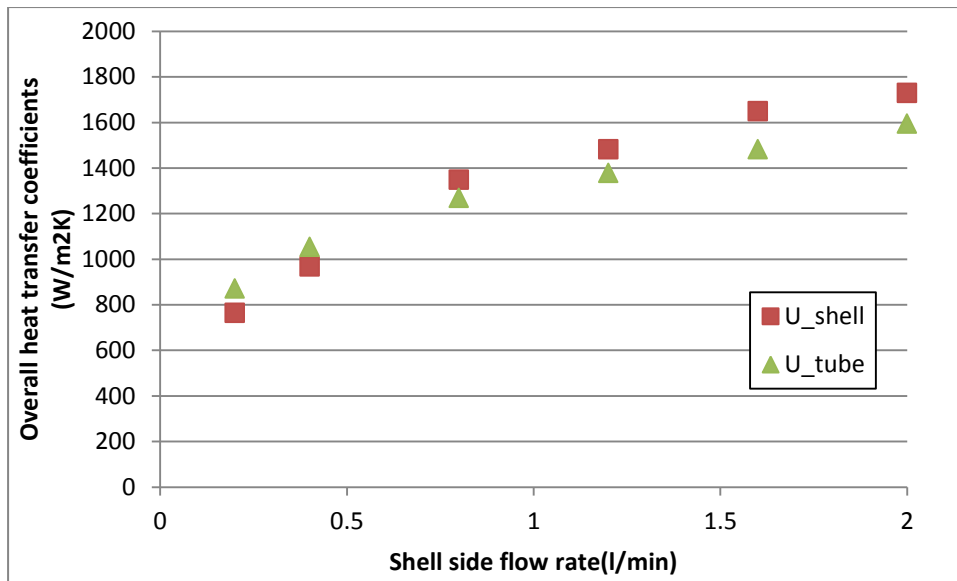


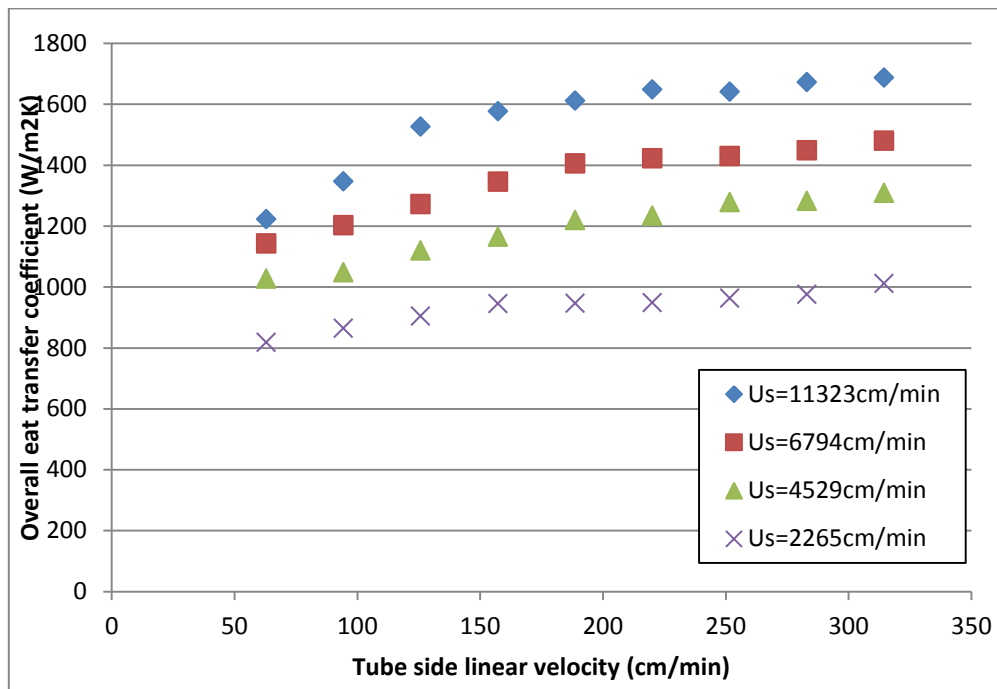
Figure 3 Experimental obtained overall heat transfer coefficients based on the shell side stream conditions and tube side stream conditions

Table 2 Representative experimental testing data for the heat transfer measurement of PHFHE

Th,i (°C)	Th,o(°C)	Tc,i (°C)	Tc,o (°C)	\dot{m}_t (l/min)	\dot{m}_s (l/min)	U_o (W/m ² K)	ϵ	NTU	HTU (cm)
Module 1 N=100									
49.4	23.9	14.9	19.0	0.3	2.0	1675	0.741	1.461	18.9
42.3	26.8	13.5	18.9	0.5	1.6	1609	0.539	0.860	26.0
51.9	41.6	15.6	35.3	0.4	0.2	767	0.711	1.235	19.7
Module 2 N=200									
69.8	43.8	15.6	39.4	0.55	0.6	857	0.478	0.884	29.3
57.1	33.5	15.2	29.6	0.55	1.0	1010	0.562	1.042	24.9
44.7	17.3	15.0	20.2	0.2	1.9	1021	0.921	2.84	15.3
Module 3 N=400									
52.0	19.2	13.9	23.4	0.5	2.0	1138	0.862	2.384	5.9
46.4	14.4	14.2	16.6	0.1	0.2	258	0.991	5.065	2.8
65.4	31.2	28.1	37.5	0.3	1.2	741	0.550	1.818	7.7

We select some typical testing data for the heat transfer measurement of PHFHE and summarize them in Table 2. These includes the hot water and cooling water inlet and outlet temperature, the mass flow rate of the two streams, the calculated total heat transfer rate, and the overall heat transfer coefficient, the heat exchanger effectiveness, the number of transfer unit (NTU) and the height of transfer unit (HTU). We can see that the overall heat transfer coefficients for such PHFHE device could reach up to 1675W/m²K for a piece of tubing with shell side diameter of 15mm and length of 14cm. In the literature³⁶, the designed value for tubular metal heat exchanger is around 1100-1400W/m²K, which is even lower than the experimental testing results of such PHFHE device. Inspection of the data in Table 2 also shows that the high value of effectiveness and NTU, up to 0.991 and 5.065 respectively, could be achieved for such PHFHE device. These values correspond to a very small HTU of

286 only 2.8cm, which is in good agreement with HTU obtained in microporous fibre membrane-
 287 based separation process³⁷.

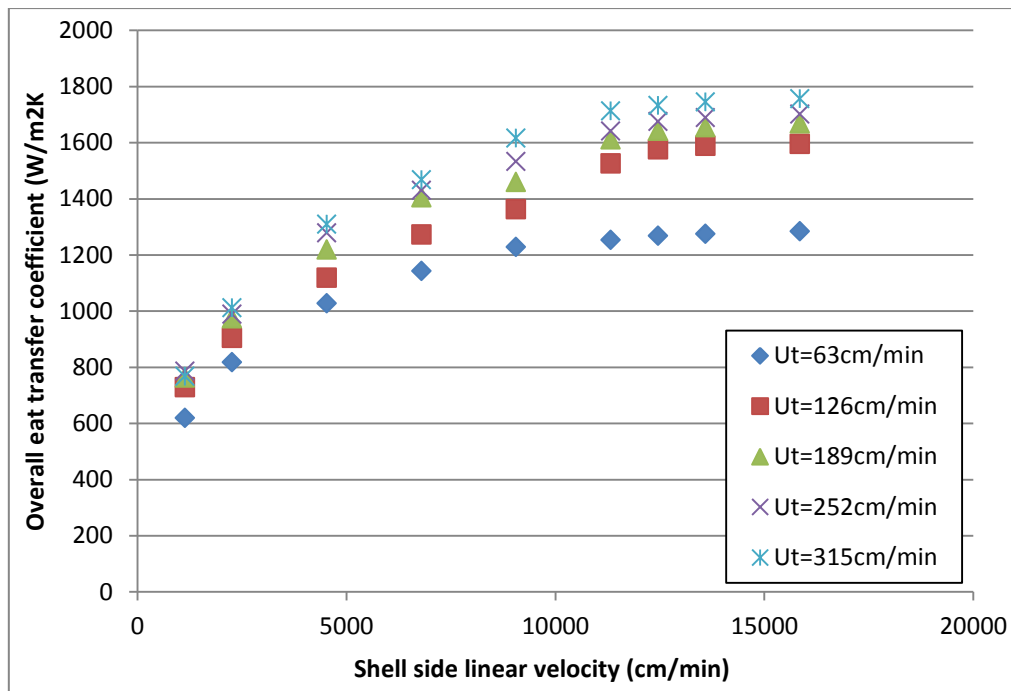


288
 289 Figure 4 Variations of experimental obtained overall heat transfer coefficients with respect to
 290 various tube side liner velocities (Module 1, hot water inlet temperature 48.5 °C)

291 In order to understand the relationship between the overall heat transfer coefficient and the
 292 fluid velocity in both shell and tube side, we present the variations of U value with tube side
 293 linear velocities when the shell side linear velocity changes from 2265cm/min to
 294 11323cm/min. We can find from Figure 4 that higher tube side linear velocity will contribute
 295 to better overall heat transfer coefficient when the shell side linear velocity is at fixed value.
 296 For instance, for shell side linear velocity at 6794cm/min, the overall heat transfer coefficient
 297 increases about 1.8% from 1405W/m²K to 1430W/m²K when the tube side linear velocity
 298 increases from 188cm/min to 252cm/min. Moreover, a common feature can be observed is
 299 that when the tube side linear velocity increases, the U value reaches a plateau quickly. The
 300 plateau U value is around 1600W/m²K for the shell side linear velocity of 11323cm/min, and
 301 1000W/m²K for the shell side linear velocity of 2265cm/min. When the tube side linear
 302 velocity is below 150cm/min, the heat transfer coefficient seems to follow a linear
 303 dependence with respect to tube side linear velocity. We can introduce Gz number to help us
 304 better understand the mechanism. According to Hewitt et al.³³, Gz is a non-dimensional group
 305 applicable mainly to transient heat conduction in laminar pipe flow. Gz represents the ratio of
 306 the time taken by heat to diffuse radially into the fluid by conduction to the time taken for the
 307 fluid to reach distance. By calculating the Gz number according to Equation (11), we can see
 308 that the Gz number is in the range of 10 to 53 when the tube side linear velocity increases
 309 from 63cm/min to 315cm/min (the same range as shown in Figure 4). As stated by Hewit et
 310 al.³³, small values of Gz (Gz < 20) indicates that radial temperature profiles are fully
 311 developed inside the laminar flow tube. This means that when Gz number and tube side linear

312 velocity are at lower values, forced convection is not the only mechanism for heat transfer,
 313 heat transfer by natural convection in the radial direction becomes more dominant.

314 Figure 5 presents the variations of U value to the various shell side linear velocities for
 315 PHFHE module 1. We can find that the U value will increase as the shell side linear velocity
 316 improves from 1132cm/min to 11320cm/min. Similarly to Figure 4, after the shell side linear
 317 velocity reaches to 11000cm/min, the U value maintains at a stale value for most of the cases.
 318 For instance, when tube side linear velocity is fixed at 126cm/min and 63cm/min, the plateau
 319 value of U is around 1600W/m²K and 1250W/m²K respectively.

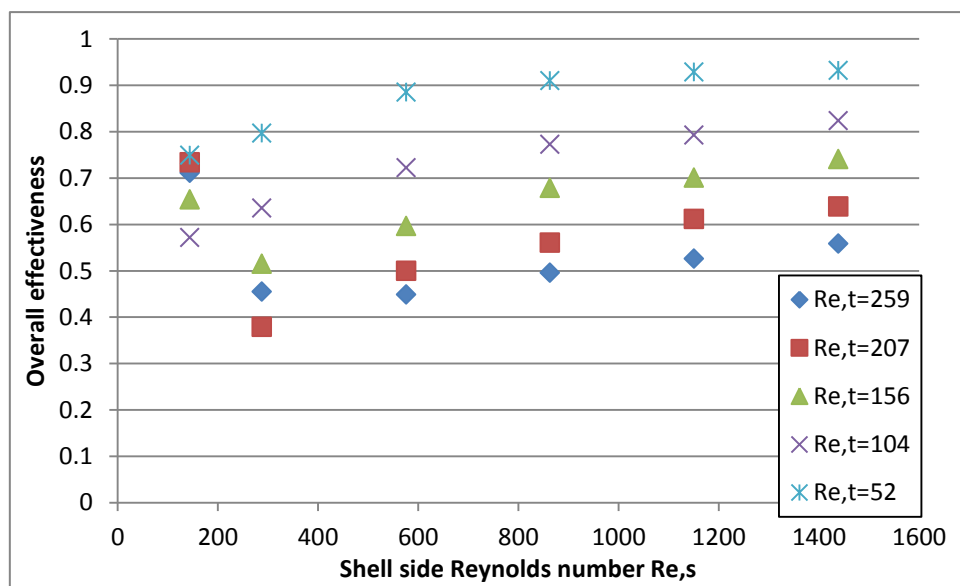


320
 321 Figure 5 Variations of experimental obtained overall heat transfer coefficients with respect to
 322 various shell side liner velocities (Module 1, hot water inlet temperature 48.5 °C)

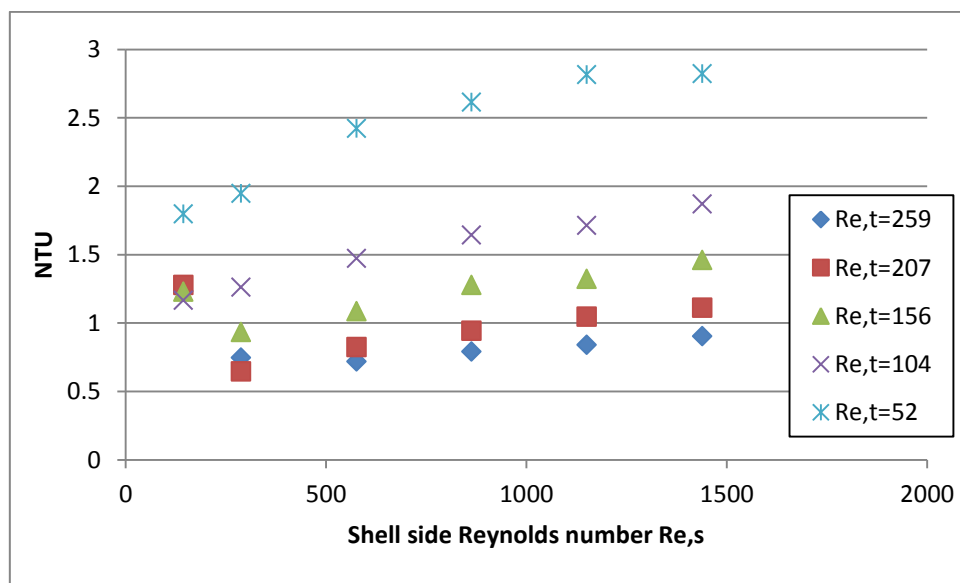
323 Figure 6-8 depict the variations of overall effectiveness, NTU and HTU of PHFHE with
 324 respect to various shell side Reynolds numbers. We can find from Figure 8 that higher shell
 325 side Reynolds number will lead to higher overall effectiveness when the tube side Reynold is
 326 at fixed value. For instance, at the tube side Reynolds number of 104, the overall
 327 effectiveness changes from 0.773 to 0.793 when the shell side Reynolds number increases
 328 from 863 to 1151. Figure 6 also reveals that at fixed shell side Reynolds number, the overall
 329 effectiveness will decrease as the tube side Reynolds number increases. For example, at shell
 330 side Reynolds number of 576, the overall effectiveness decreases from 0.597 to 0.5 when the
 331 tube side Reynolds number increases from 156 to 207. Figure 7 shows that for most of the
 332 cases (about 83%), the NTU is higher than 1. As the PHFHE device mainly operates in
 333 laminar flow regime, Figure 7 also reveals that high NTU can be obtained at low tube side
 334 Reynolds number, which is in good agreement with the heat transfer literature³⁸. Inspection
 335 of Figure 6 and 7 also shows that, the overall effectiveness first decreases and then increases
 336 as the shell side Re number improves. The reason is because that, according to Eq. (5), the
 337 effectiveness is proportional related to C_{min} , which is the minimum product of the flow rate

338 multiple by C_p for shell side and tube side. At lower shell side Re number ($Re_s = 144$) and
 339 higher tube side Re number ($Re_t > 156$), the effect of shell side flow rate on the effectiveness
 340 is more dominant. As the shell side Re number becomes higher than the tube side Re number,
 341 the effectiveness is more dependent on tube side Re number. That is why there is a small
 342 fluctuation at lower shell side Re number.

343 From Figure 6-8, we can see that high value of heat exchanger effectiveness and NTU, 0.932
 344 and 0.822 respectively, could be achieved at the tube side Reynolds number of 52 and shell
 345 side Reynolds of 1439. However, inspection of Figure 6-8 further indicates that relatively low
 346 effectiveness and NTU values, accompanied by high HTU also exist. This means that the
 347 rating of the PHFHE device is rather important. In order to achieve higher effectiveness and
 348 better thermal performance, the rating of PHFHE device should be performed properly.

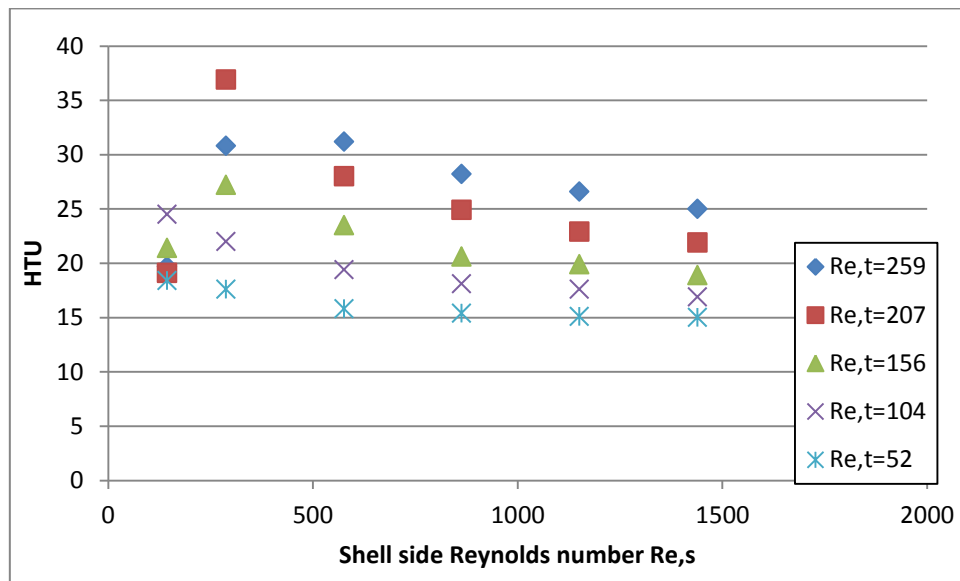


349
 350 Figure 6 Variations of overall effectiveness with respect to various shell side Reynolds
 351 number (Module 1, hot water inlet temperature 48.5 °C)



352

353 Figure 7 Variations of NTU with respect to various shell side Reynolds number (Module 1,
 354 hot water inlet temperature 48.5 °C)

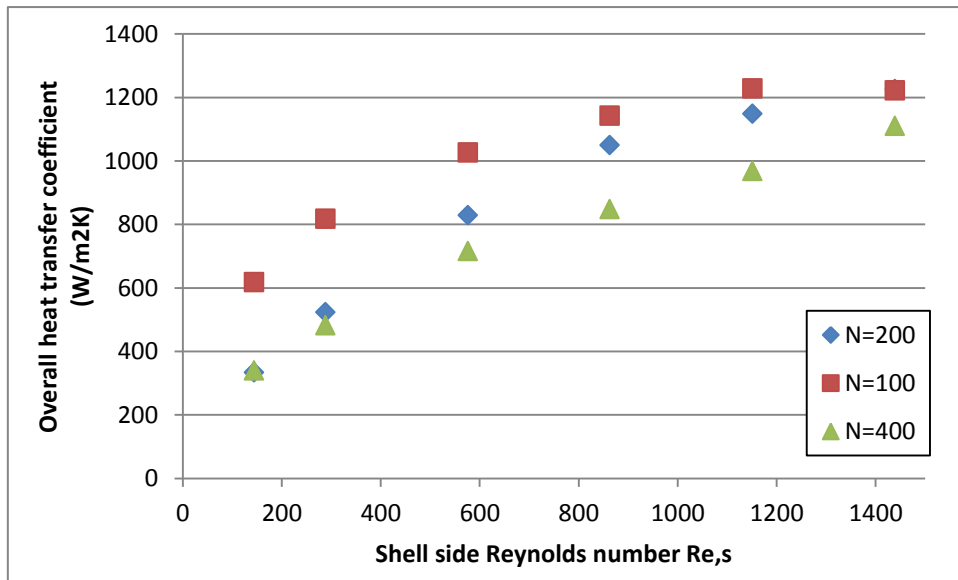


355
 356 Figure 8 Variations of HTU with respect to various shell side Reynolds number (Module 1,
 357 hot water inlet temperature 48.5 °C)

358 Figure 9-11 show the comparisons of overall heat transfer coefficients, heat transfer rate and
 359 LMTD for different fibre numbers under various shell side Reynolds numbers, at fixed tube
 360 side Reynolds number. It can be found that at the same shell and tube side Reynolds number,
 361 the module with smaller fibre number produces higher overall heat transfer coefficient. For
 362 instance, at shell side Reynolds number of 288, the overall heat transfer coefficient decreases
 363 from 817.6 W/m²K to 523.5 W/m²K, till 481.9 W/m²K as the fibre number changes from 100,
 364 200 to 400. The reason can be referred to Equation (2), the U value is closely related to the
 365 total heat transfer rate Q, ΔT_{lm} , and the heat transfer area A. As shown in Figure 10, at shell
 366 side Reynolds number of 288, when the fibre number increases from 100 to 200, the total
 367 heat transfer rate increases about 29.1% from 214.8W to 277.3W. Figure 11 indicates that at
 368 the same condition, ΔT_{lm} decreases about 0.7% from 11.6 °C to 9.9°C, as the fibre number
 369 increases from 100 to 200. In the meantime, the total heat transfer area improves twice as the
 370 fibre number increase from 100 to 200. Compares the abovementioned percentage difference,
 371 we can see that the change of fibre numbers plays more dominant role on the overall heat
 372 transfer coefficients. Therefore, the increase of fibre number will lead to the decrease of
 373 overall U value. This is also the reason as U value decreases when the fibre number increases
 374 with the variations of tube side Reynolds number, as shown in Figure 12.

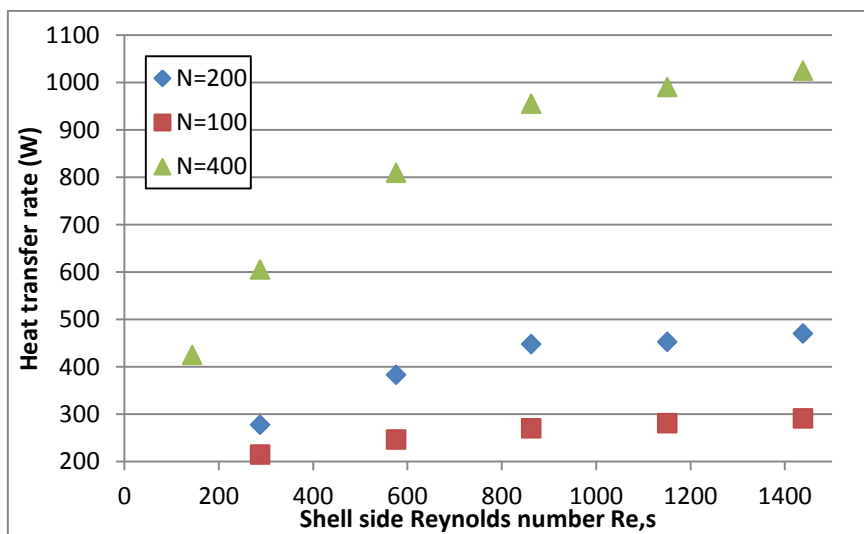
375 Inspection of Figure 9 -11 further reveals an interesting phenomenon: at lower shell side flow
 376 rate, the heat transfer rate stays very close for N=200 and N=100, while there is a much
 377 bigger difference for N=400 and N=200. For instance, at shell side Re number of 288, the Q
 378 value increases about 29.1% from 214.8 W/m²K to 277.3W as the fibre number increases
 379 from 100 to 200, while it soars about 64.2% from 277.3W to 605.6W as the fibre number
 380 improves from 200 to 400. On the other hand, at lower shell side flow rate, the overall heat

381 transfer rate for N=200 and N=400 are approaching each other, while there is a big gap
 382 between N=100 and N=200. Hence, when we design the PHFHE device, the fibre numbers
 383 should be selected properly in order to maintain effective heat transfer while making full uses
 384 of the fibre materials.



385

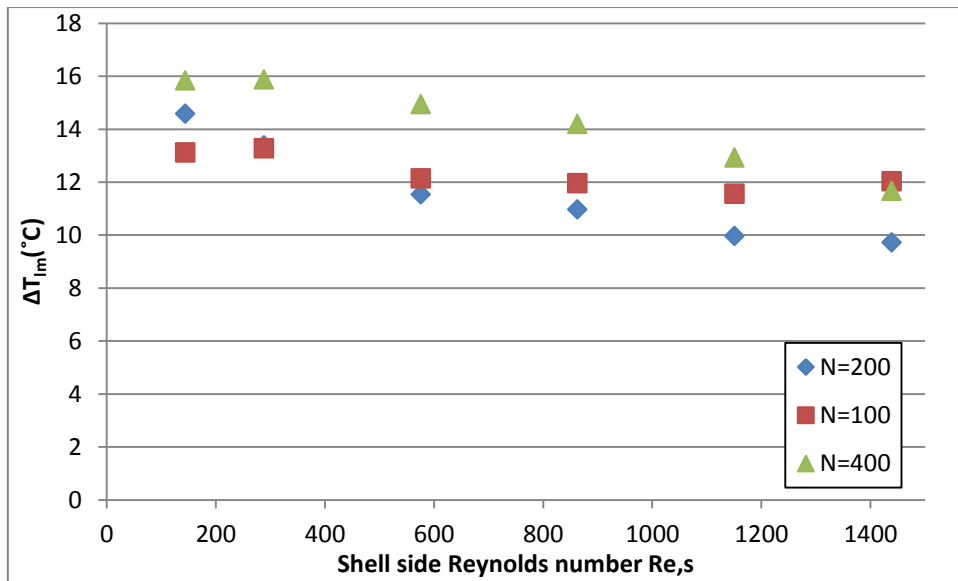
386 Figure 9 Comparisons of overall heat transfer coefficients for Module 1-3 under various shell
 387 side flow rate and at fixed tube side Reynolds number



388

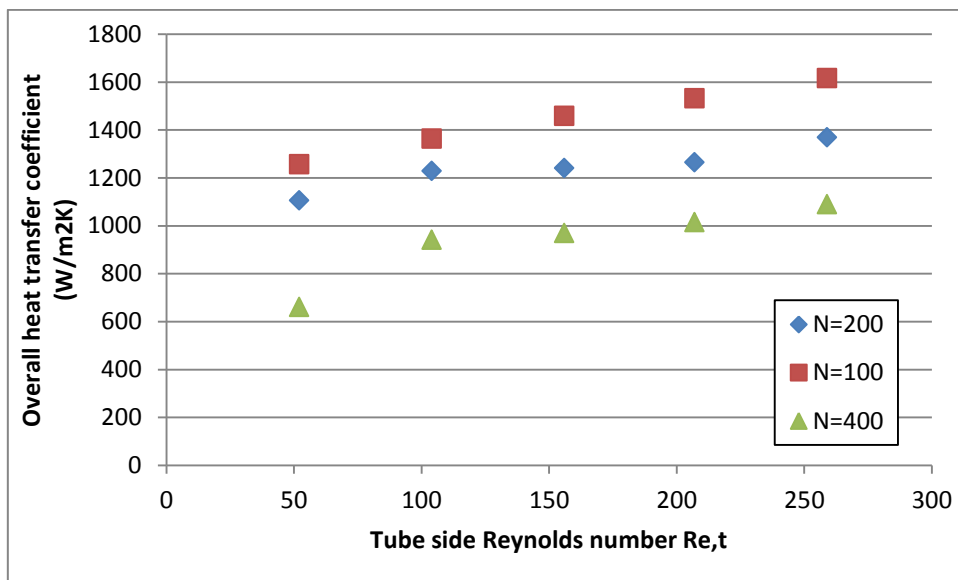
389 Figure 10 Comparisons of heat transfer rate for Module 1-3 under various shell side flow rate
 390 and at fixed tube side Reynolds number

391



392

393 Figure 11 Comparisons of ΔT_{lm} for Module 1-3 under various shell side flow rate and at fixed
 394 tube side Reynolds number



395

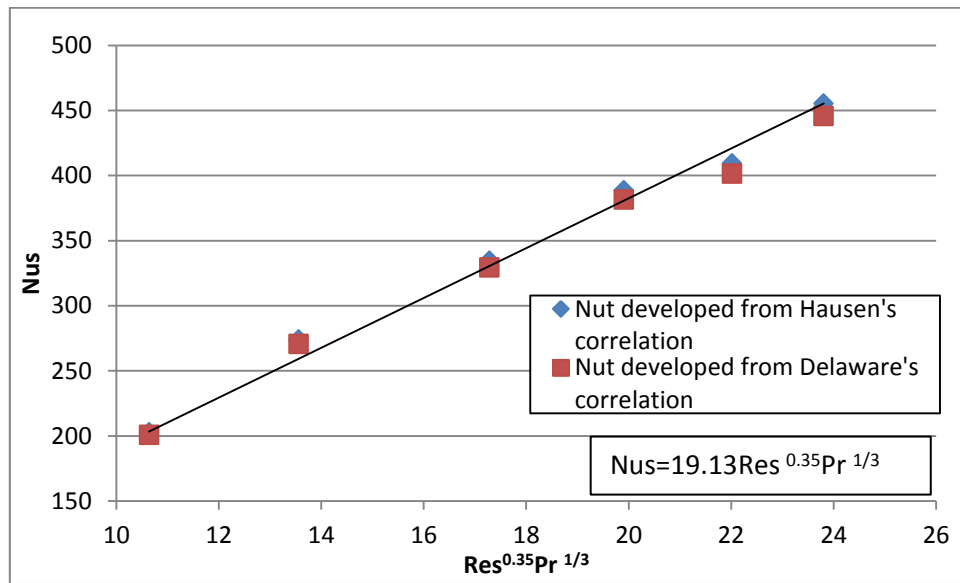
396 Figure 12 Comparisons of overall heat transfer coefficients for Module 1-3 under various
 397 tube side flow rate and at fixed shell side flow rate of 1.6l/min

398 Table 3 Percentage contribution of tube side, shell side and fibre wall resistance to the overall
 399 resistance

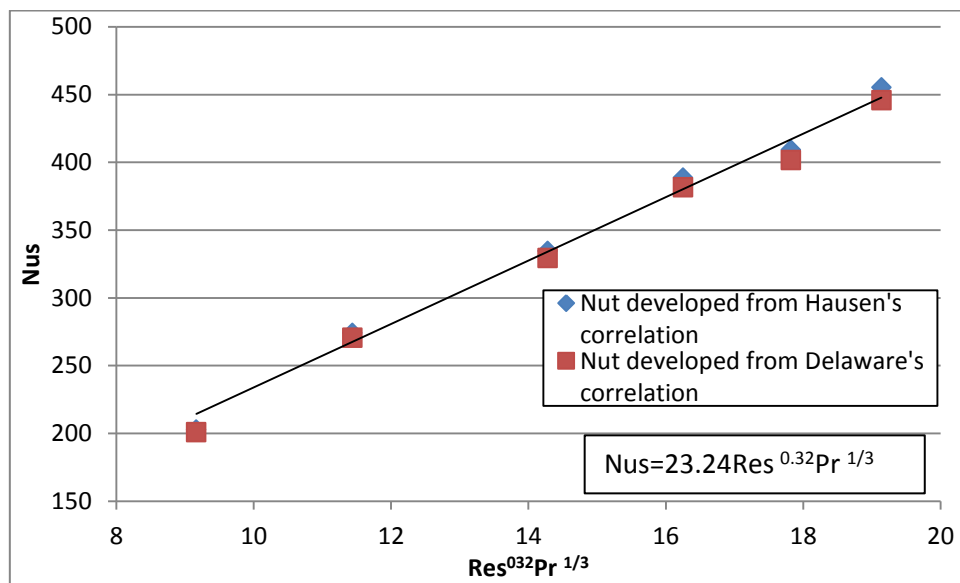
Module	Fibre number	R_t/R_{ov} (%)	R_s/R_{ov} (%)	R_w/R_{ov} (%)
1	100	4-10	35-56	18-31
2	200	3-8	38-62	15-28
3	400	2-7	40-66	13-25

400 Table 3 presents the percentage contribution of the three major resistances to the overall
 401 resistance. The results indicate that tube side resistance are the smallest of the three, therefore
 402 by increasing the tube-side Reynolds number, little improvement will be achieved for the

403 overall heat transfer performance. By increasing the fibre numbers from 100, 200 to 400, the
 404 overall heat transfer coefficients tend to decrease accordingly, and the percentage
 405 contribution of shell side resistance will play more dominant role.



406
 407 Figure 13 Shell side Nu numbers with respect to Re and Pr number using two different
 408 correlations (correlation 1)

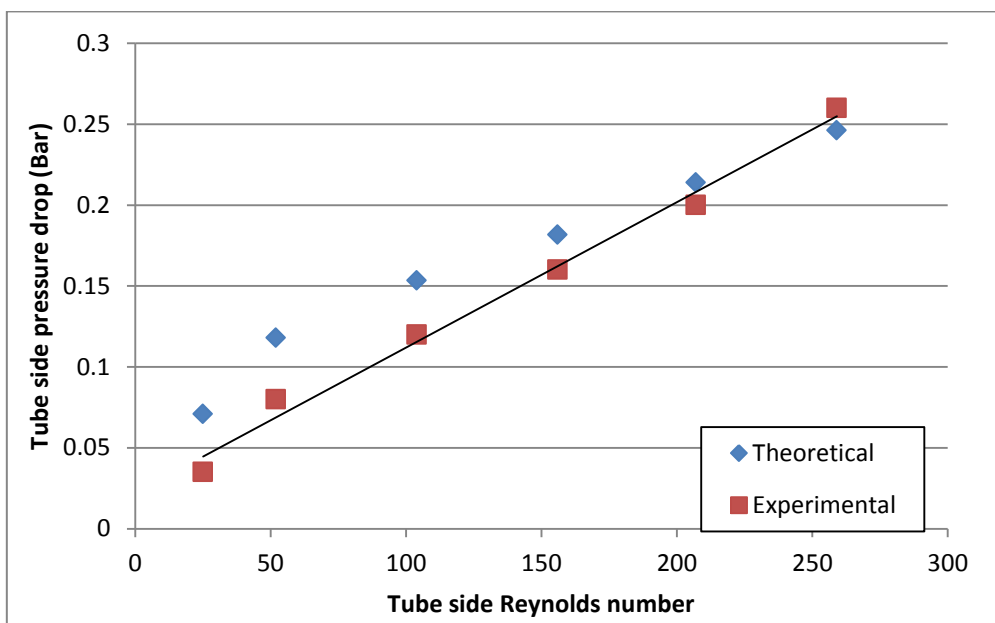


409
 410 Figure 14 Shell side Nu numbers with respect to Re and Pr number using two different
 411 correlations (correlation 2)

412 Figure 13 and Figure 14 present the relationships between shell side Nu numbers and Re, Pr
 413 number using two different correlations from the literature. Both suitable for laminar flow
 414 conditions and validated by various authours³⁹⁻⁴¹, Hausen's correlation⁴² and Delaware's
 415 correlation³⁵ were applied respectively for calculating the tube side heat transfer coefficients.
 416 Then, the shell side heat transfer coefficients and the shell side Nu number could be derived
 417 from the experimental obtained overall heat transfer coefficients. The Nu-Re plot shown in

418 Figure 13 and Figure 14 indicated very good agreement of shell side Nu numbers using two
 419 different correlations. A well correlated equation showing shell side Nu number as the
 420 function of Re and Pr number is also presented respectively in Figure 13 and Figure 14. The
 421 difference between the correlation presented in Figure 13 and Figure 14 is the exponent of
 422 shell side Re number. Comparing the discrepancy of the correlated equation with results
 423 obtained from Hausen's and Delaware correlations, it can be found that the derived
 424 correlation 1 with exponent of 0.35(in Figure 13) is more suitable for shell side Re number
 425 less than 200 or larger than 1200, with the minimum difference of 0.3%. While the derived
 426 correlation 2 with exponent of 0.32(in Figure 14) is more close to results obtained from
 427 Hausen's and Delaware correlations (with the minimum difference of 0.14%), when the shell
 428 side Re number is in the range of 200-1200.

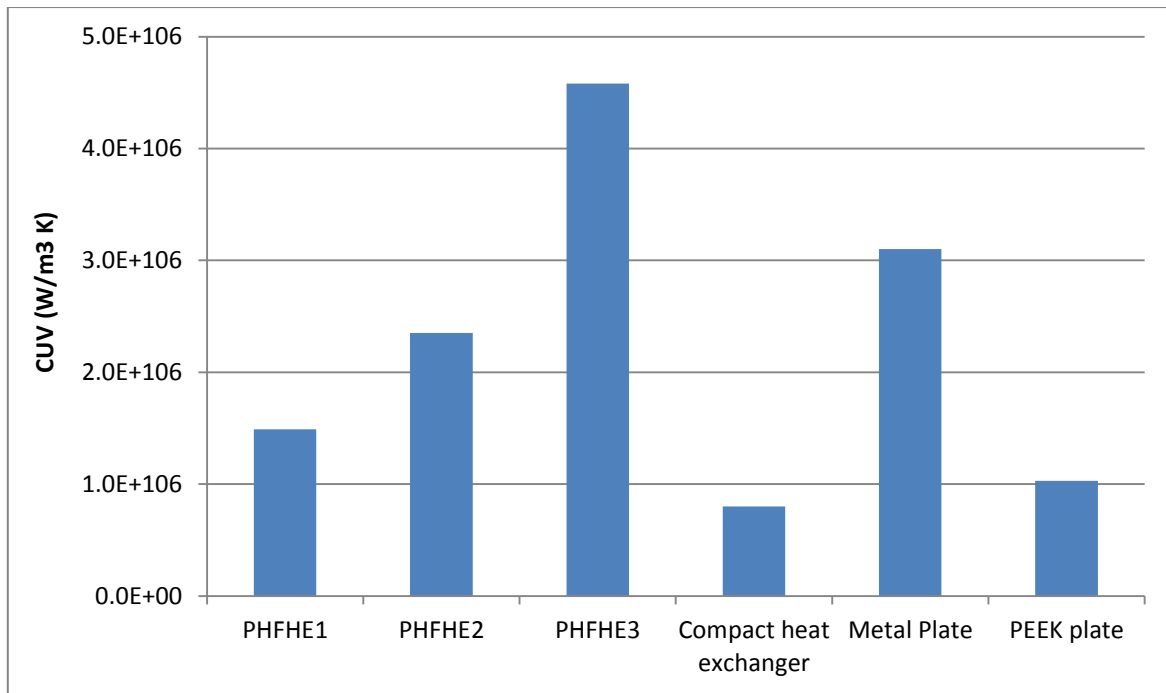
429



430

431 Figure 15 Variations of theoretical and experimental obtained tube side pressure drops under
 432 different tube side Re numbers. (Module 1)

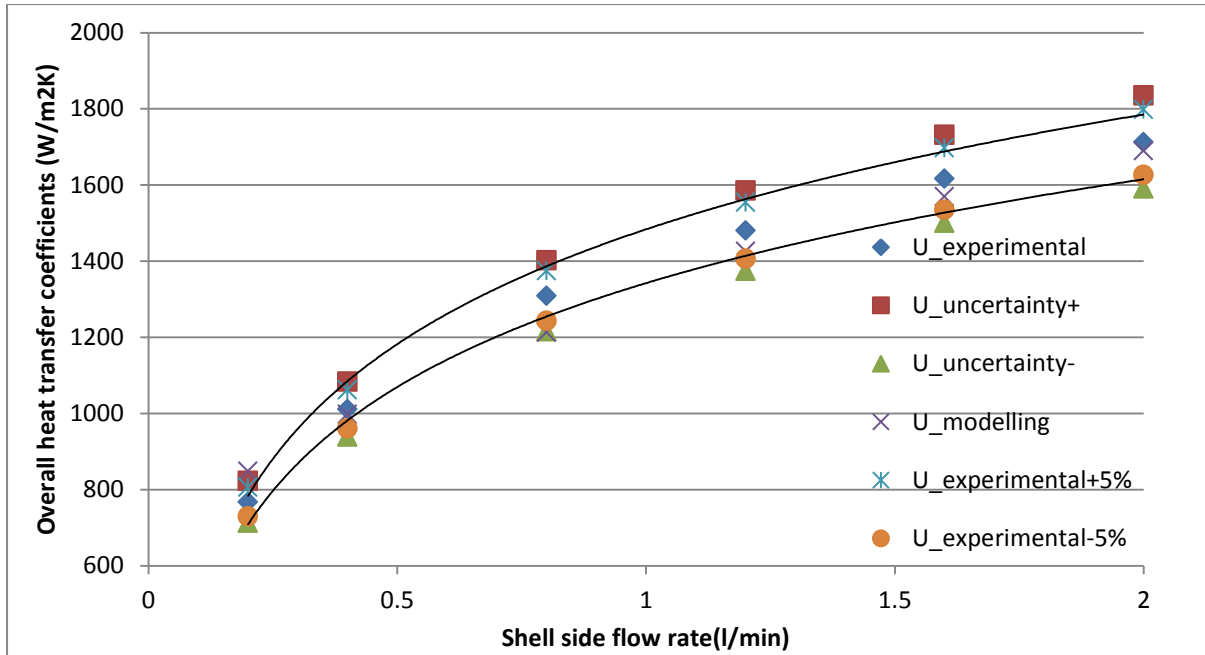
433 Figure 15 shows the comparisons of theoretical and experimental obtained tube side pressure
 434 drops under different tube side Re numbers for fibre number N=100. The theoretical tube side
 435 pressure drop is calculated using Eq. (12). The experimental tube side pressures of PHFHE
 436 are monitored by pressured transducer sensors (GE UNIK 5000). We can see from the
 437 diagram that increasing the tube side Re number will result in higher tube side pressure drop.
 438 Moreover, a liner relationship could be derived between experimental obtained Re number
 439 and tube side pressure drop with $R^2=0.99$. We can also find that the experimental obtained
 440 pressure drops are quite close to the theoretical values, with the minimum percentage
 441 difference of 5.6%. As the tube sider Re number increase, the difference between the
 442 theoretical and experimental results decreases.



443

444 Figure 16 Comparisons of overall conductance per unit volume between PHFHE with
 445 conventional heat exchangers

446 Figure 16 shows the comparisons of overall conductance per unit volume between PHFHEs
 447 with conventional metal and plastic heat exchangers. A compact metal heat exchanger with
 448 wall thickness of 0.4mm⁴³, a plate heat exchanger with 0.4mm thickness³⁶, and a PEEK plate
 449 heat exchanger¹⁷ are chosen for comparisons. We can see from Figure 15 that PHFHE
 450 modules generally demonstrate higher CUV values (about 2-8 times) compared with
 451 conventional metal and plastic heat exchangers. Despite the relatively low overall heat
 452 transfer coefficients, the large surface area to volume ratio of PHFHEs offers controlling
 453 factor of performance on a volumetric basis. For instance, for PHFHE module 3 (fibre
 454 number=400), the CUV values are about 7 times higher than the compact tube heat
 455 exchanger⁴³, and 1.5 times higher than the metal plate heat exchanger³⁶. However, the values
 456 in Figure 16 for the metal heat exchangers already represent the cutting edge of current
 457 technology. While the packing/manufacturing technology for the PHFHEs are currently only
 458 subjected to laboratory testing conditions. Hence, we could expect more area to be packed in
 459 the PHFHEs, and this will result in even better heat transfer performance and thermal
 460 capabilities, which exceeds greatly over the metal counterparts.



461

462 Figure 17 Comparisons of overall heat transfer coefficients obtained from experiments,
 463 uncertainty calculations and the modelling results

464 The uncertainty analysis of the experimental results shown in Figure 17 is performed using
 465 the methods proposed by Moffat⁴⁴. Considering all the measurement uncertainties for mass
 466 flow rates, temperatures, and fibre diameters, the experimental uncertainties for the overall
 467 heat transfer coefficients is between $\pm 7.1\%$ and $\pm 9.8\%$. Based on the experimental inlet and
 468 outlet streams conditions, the simulation programme developed by the authors was applied
 469 and results are presented in Figure 15. We also plot two curves showing the deviations of $\pm 5\%$
 470 from the experimental obtained results. We can find that, in general, the simulation results
 471 fall in good agreement with the experimental data, with differences less than 5%.

472 **5. Conclusion**

473 The PP based polymer hollow fibre heat exchangers were manufactured and tested under
 474 various shell (0.2-2.0l/min), tube side flow rate (0.1-0.6l/min) and tube side water
 475 temperatures (40-70°C). The maximum experimental obtained overall heat transfer
 476 coefficients were achieved in module 1 of PHFHE, with the U values between 1700-
 477 1800W/m²K. These values are higher than other results reported in literature for water to
 478 water applications in polymer hollow fibre heat exchanger.

479 Three different PHFHE modules with fibre numbers of 100, 200 and 400 were manufactured
 480 and the thermal performances were compared in the tests. The experimental obtained overall
 481 heat transfer coefficients were 758-1675W/m²K, 369-1453W/m²K and 296-1201W/m²K
 482 respectively for Module 1, 2 and 3. This indicates that module 1 offers higher U value
 483 compared with the other two modules.

484 By changing the tube and shell side flow rate, the effectiveness, NTU and HTU of PHFHE
 485 modules are also investigated. With the active length of 14cm, the module 1 of PHFHE could

486 attain high value of effectiveness and NTU, up to 0.991 and 5.065 respectively. The HTU
487 achieved was as low as 2.8cm, about 35 times less than the lower limit for shell and tube heat
488 exchangers and 20 times lower than typical values for plate heat exchangers. Such results
489 demonstrate that if PHFHE devices could be rated and designed properly, they could achieve
490 relatively high NTU in a single module.

491 Since the surface area per unit volume in such PHFHEs is quite high, in the range of 880-
492 3600 m²/m³, their volumetric rate of heat transfer is very high. Comparisons of CUV between
493 PHFHEs and metal heat exchangers reveals that the CUV values of PHFHEs are
494 approximately 2-7 times higher than the metal counterparts. This superior performance can
495 result in potentially more compact designs based on PHFHE devices, for water desalination,
496 solar water heating system, and automotive applications. Therefore, the superior thermal
497 performance, and large heat transfer areas, and the advantages of low price and light weight
498 of polymer materials, make PHFHEs a promising substitute over conventional metal heat
499 recovery system for building application.

500 **Acknowledgement**

501 The authors would like to acknowledge the financial support and contributions from Innovate
502 UK (project code: 131821).

503 **Reference**

- 504 1 Pérez-Lombard, L., Ortiz, J. & Pout, C. A review on buildings energy consumption information.
505 *Energy and Buildings* **40**, 394-398, doi:<http://dx.doi.org/10.1016/j.enbuild.2007.03.007>
506 (2008).
- 507 2 Mardiana-Idayu, A. & Riffat, S. B. Review on heat recovery technologies for building
508 applications. *Renewable and Sustainable Energy Reviews* **16**, 1241-1255,
509 doi:<http://dx.doi.org/10.1016/j.rser.2011.09.026> (2012).
- 510 3 Shao, L., Riffat, S. B. & Gan, G. Heat recovery with low pressure loss for natural ventilation.
511 *Energy and Buildings* **28**, 179-184, doi:[http://dx.doi.org/10.1016/S0378-7788\(98\)00016-4](http://dx.doi.org/10.1016/S0378-7788(98)00016-4)
512 (1998).
- 513 4 Zhou, Y. P., Wu, J. Y. & Wang, R. Z. Performance of energy recovery ventilator with various
514 weathers and temperature set-points. *Energy and Buildings* **39**, 1202-1210,
515 doi:<http://dx.doi.org/10.1016/j.enbuild.2006.12.010> (2007).
- 516 5 Roulet, C. A., Heidt, F. D., Foradini, F. & Pibiri, M. C. Real heat recovery with air handling
517 units. *Energy and Buildings* **33**, 495-502, doi:[http://dx.doi.org/10.1016/S0378-7788\(00\)00104-3](http://dx.doi.org/10.1016/S0378-7788(00)00104-3) (2001).
- 519 6 Nasif, M., Al-Waked, R., Morrison, G. & Behnia, M. Membrane heat exchanger in HVAC
520 energy recovery systems, systems energy analysis. *Energy and Buildings* **42**, 1833-1840,
521 doi:<http://dx.doi.org/10.1016/j.enbuild.2010.05.020> (2010).
- 522 7 Mahmud, K., Mahmood, G. I., Simonson, C. J. & Besant, R. W. Performance testing of a
523 counter-cross-flow run-around membrane energy exchanger (RAMEE) system for HVAC
524 applications. *Energy and Buildings* **42**, 1139-1147,
525 doi:<http://dx.doi.org/10.1016/j.enbuild.2010.02.005> (2010).
- 526 8 Manz, H. & Huber, H. Experimental and numerical study of a duct/heat exchanger unit for
527 building ventilation. *Energy and Buildings* **32**, 189-196, doi:[http://dx.doi.org/10.1016/S0378-7788\(00\)00043-8](http://dx.doi.org/10.1016/S0378-7788(00)00043-8) (2000).

- 529 9 Kragh, J., Rose, J., Nielsen, T. R. & Svendsen, S. New counter flow heat exchanger designed
530 for ventilation systems in cold climates. *Energy and Buildings* **39**, 1151-1158,
531 doi:<http://dx.doi.org/10.1016/j.enbuild.2006.12.008> (2007).
- 532 10 Dartnall, W. J., Revel, A. & Giotis, V. Air-Conditioning Employing Indirect Evaporative Cooling
533 Can Be Shown to Derive Its Energy From the Solar Source. *ASME Proceedings | Energy*
534 *Systems: Analysis, Thermodynamics and Sustainability, November 2009, Florida, USA* (2009).
- 535 11 Kachhwaha, S. S. & Prabhakar, S. Heat and mass transfer study in a direct evaporative cooler.
536 *Journal of Scientific & Industrial Research* **69**, 705-710 (2010).
- 537 12 Bahadur, R. & Bar-Cohen, A. Thermal design and optimization of natural convection polymer
538 pin fin heat sinks. *Components and Packaging Technologies, IEEE Transactions on* **28**, 238-
539 246 (2005).
- 540 13 Bahadur, R. & Bar-Cohen, A. in *Thermal and Thermomechanical Phenomena in Electronic*
541 *Systems, 2004. ITherm'04. The Ninth Intersociety Conference on*. 268-275 (IEEE).
- 542 14 Song, L., Li, B., Zarkadas, D., Christian, S. & Sirkar, K. K. Polymeric hollow-fiber heat
543 exchangers for thermal desalination processes. *Industrial and Engineering Chemistry*
544 *Research* **49**, 11961-11977, doi:10.1021/ie100375b (2010).
- 545 15 Bourouni, K., Martin, R., Tadrict, L. & Tadrict, H. Experimental investigation of evaporation
546 performances of a desalination prototype using the aero-evapo-condensation process.
547 *Desalination* **114**, 111-128, doi:[http://dx.doi.org/10.1016/S0011-9164\(98\)00003-4](http://dx.doi.org/10.1016/S0011-9164(98)00003-4) (1997).
- 548 16 Wu, C., Mantell, S. C. & Davidson, J. Polymers for solar domestic hot water: Long-term
549 performance of PB and nylon 6, 6 tubing in hot water. *Journal of solar energy engineering*
550 **126**, 581-586 (2004).
- 551 17 Liu, W., Davidson, J. & Mantell, S. Thermal analysis of polymer heat exchangers for solar
552 water heating: A case study. *Journal of Solar Energy Engineering, Transactions of the ASME*
553 **122**, 84-91 (2000).
- 554 18 Huang, S.-M., Zhang, L.-Z., Tang, K. & Pei, L.-X. Turbulent Heat and Mass Transfer Across a
555 Hollow Fiber Membrane Tube Bank in Liquid Desiccant Air Dehumidification. *Journal of Heat*
556 *Transfer* **134**, 082001-082001, doi:10.1115/1.4006208 (2012).
- 557 19 Zhang, L.-Z., Huang, S.-M. & Pei, L.-X. Conjugate heat and mass transfer in a cross-flow
558 hollow fiber membrane contactor for liquid desiccant air dehumidification. *International*
559 *Journal of Heat and Mass Transfer* **55**, 8061-8072,
560 doi:<http://dx.doi.org/10.1016/j.ijheatmasstransfer.2012.08.041> (2012).
- 561 20 Chen, X., Su, Y., Reay, D. & Riffat, S. Recent research developments in polymer heat
562 exchangers – A review. *Renewable and Sustainable Energy Reviews* **60**, 1367-1386,
563 doi:<http://dx.doi.org/10.1016/j.rser.2016.03.024> (2016).
- 564 21 El-Dessouky, H. T. & Ettouney, H. M. Plastic/compact heat exchangers for single-effect
565 desalination systems. *Desalination* **122**, 271-289, doi:[http://dx.doi.org/10.1016/S0011-](http://dx.doi.org/10.1016/S0011-9164(99)00048-X)
566 [9164\(99\)00048-X](http://dx.doi.org/10.1016/S0011-9164(99)00048-X) (1999).
- 567 22 Hetsroni, G. & Mosyak, A. Heat transfer and pressure drop in a plastic heat exchanger with
568 triangular channels. *Chemical Engineering and Processing: Process Intensification* **33**, 91-100,
569 doi:[http://dx.doi.org/10.1016/0255-2701\(94\)85007-0](http://dx.doi.org/10.1016/0255-2701(94)85007-0) (1994).
- 570 23 Wharry Jr, S. R. Fluoropolymer heat exchangers. *Metal Finishing* **93**, 693-704,
571 doi:[http://dx.doi.org/10.1016/0026-0576\(95\)93415-X](http://dx.doi.org/10.1016/0026-0576(95)93415-X) (1995).
- 572 24 Brouwers, H. J. H. & Van Der Geld, C. W. M. Heat transfer, condensation and fog formation
573 in crossflow plastic heat exchangers. *International Journal of Heat and Mass Transfer* **39**,
574 391-405, doi:[http://dx.doi.org/10.1016/0017-9310\(95\)00113-N](http://dx.doi.org/10.1016/0017-9310(95)00113-N) (1996).
- 575 25 Bandelier, P., Deronzier, J. C. & Lauro, F. Plastic heat exchangers. *Matériaux & Techniques* **9-**
576 **10**, 67-70 (1992).
- 577 26 Bourouni, K., Martin, R., Tadrict, L. & Chaibi, M. T. Heat transfer and evaporation in
578 geothermal desalination units. *Applied Energy* **64**, 129-147,
579 doi:[http://dx.doi.org/10.1016/S0306-2619\(99\)00071-9](http://dx.doi.org/10.1016/S0306-2619(99)00071-9) (1999).

- 580 27 Zarkadas, D. M., Li, B. & Sirkar, K. K. in *Proceedings of the ASME Summer Heat Transfer*
581 *Conference*. 429-438.
- 582 28 Yang, D. *et al.* Hollow fibers as structured packing for olefin/paraffin separations. *Journal of*
583 *membrane science* **279**, 61-69 (2006).
- 584 29 Yang, D., Le, L., Martinez, R. & Morrison, M. Hollow fibers structured packings in
585 olefin/paraffin distillation: apparatus scale-up and long-term stability. *Industrial &*
586 *Engineering Chemistry Research* **52**, 9165-9179 (2013).
- 587 30 Astrouski I., Raudensky M. & M., D. Particulate fouling of polymeric hollow fiber heat
588 exchanger. *Proceedings of international conference on heat exchanger fouling and cleaning,*
589 *June 09-14, 2013, Budapest, Hungary* (2013).
- 590 31 Zhao, J. *et al.* Numerical simulation of novel polypropylene hollow fiber heat exchanger and
591 analysis of its characteristics. *Applied Thermal Engineering* **59**, 134-141,
592 doi:<http://dx.doi.org/10.1016/j.applthermaleng.2013.05.025> (2013).
- 593 32 Shah, R. K. Heat exchanger basic design methods. In *Low Reynolds number flow heat*
594 *exchangers*, Hemisphere Publishing Co. New York (1983).
- 595 33 Hewitt, G. F., Shires, G. L. & Bott, T. R. Process Heat Transfer. *CRC Press, Boca Raton, FL, USA.*
596 (1994).
- 597 34 Mohiuddin Mala, G. & Li, D. Flow characteristics of water in microtubes. *International*
598 *Journal of Heat and Fluid Flow* **20**, 142-148, doi:[http://dx.doi.org/10.1016/S0142-](http://dx.doi.org/10.1016/S0142-727X(98)10043-7)
599 [727X\(98\)10043-7](http://dx.doi.org/10.1016/S0142-727X(98)10043-7) (1999).
- 600 35 Kern, D. Q. Process Heat Transfer. *Mcgraw-Hill College; 1St Edition edition* (1950).
- 601 36 Don W. Green & Perry, R. H. Perry's Chemical Engineers' Handbook, Eighth Edition. *McGraw-*
602 *Hill Professional, New York, 2007* (2007).
- 603 37 Prasad, R. & Sirkar, K. Dispersion - free solvent extraction with microporous hollow - fiber
604 modules. *AIChE journal* **34**, 177-188 (1988).
- 605 38 Schlundler, E. U. Heat exchanger deisgn handbook. *Hemisphere Publishing Co., New York, NY*
606 (1983).
- 607 39 Chen, L., Sun, Y., Du, X., Wei, G. & Yang, L. Performance Analysis of Anti-corrosion Heat
608 Exchangers Made of Special Plastics for Flue Gas Heat Recovery. *Proceedings of the CSEE* **34**,
609 2778-2783 (2014).
- 610 40 Zhang, L.-Z. & Huang, S.-M. Coupled heat and mass transfer in a counter flow hollow fiber
611 membrane module for air humidification. *International Journal of Heat and Mass Transfer* **54**,
612 1055-1063, doi:<http://dx.doi.org/10.1016/j.ijheatmasstransfer.2010.11.025> (2011).
- 613 41 Lv, Y., Yu, X., Tu, S.-T., Yan, J. & Dahlquist, E. Experimental studies on simultaneous removal
614 of CO₂ and SO₂ in a polypropylene hollow fiber membrane contactor. *Applied Energy* **97**,
615 283-288, doi:<http://dx.doi.org/10.1016/j.apenergy.2012.01.034> (2012).
- 616 42 Karlsson, H. O. E. & Trägårdh, G. Heat transfer in pervaporation. *Journal of Membrane*
617 *Science* **119**, 295-306, doi:[http://dx.doi.org/10.1016/0376-7388\(96\)00150-0](http://dx.doi.org/10.1016/0376-7388(96)00150-0) (1996).
- 618 43 Taler, D. Prediction of heat transfer correlations for compact heat exchangers. *Forschung im*
619 *Ingenieurwesen* **69**, 137-150, doi:10.1007/s10010-004-0148-5.
- 620 44 Moffat, R. J. Describing the uncertainties in experimental results. *Experimental Thermal and*
621 *Fluid Science* **1**, 3-17, doi:[http://dx.doi.org/10.1016/0894-1777\(88\)90043-X](http://dx.doi.org/10.1016/0894-1777(88)90043-X) (1988).

622